NASA TECHNICAL MEMORANDUM

UB
NASA TM X-1669

UB
NASA TM X-1669

FLIGHT EXPERIENCE WITH SHOCK IMPINGEMENT AND INTERFERENCE HEATING ON THE X-15-2 RESEARCH AIRPLANE

by Joe D. Watts

Flight Research Center
Edwards, Calif.

NATIONAL AERONAUTICS AND SPACE ADMINISTRATION • WASHINGTON, D. C. • OCTOBER 1968

NASA TM X-1669

FLIGHT EXPERIENCE WITH SHOCK IMPINGEMENT AND INTERFERENCE HEATING ON THE X-15-2 RESEARCH AIRPLANE

By Joe D. Watts

Flight Research Center
Edwards, Calif.

GROUP 4
Downgraded at 3 year intervals;
declassified after 12 years

CLASSIFIED DOCUMENT–TITLE UNCLASSIFIED
This material contains information affecting the national defense of the United States within the meaning of the espionage laws, Title 18, U.S.C., Secs. 793 and 794, the transmission or revelation of which in any manner to an unauthorized person is prohibited by law.

NOTICE
This document should not be returned after it has satisfied your requirements. It may be disposed of in accordance with your local security regulations or the appropriate provisions of the Industrial Security Manual for Safe-Guarding Classified Information.

NATIONAL AERONAUTICS AND SPACE ADMINISTRATION

FLIGHT EXPERIENCE WITH SHOCK IMPINGEMENT AND INTERFERENCE HEATING ON THE X-15-2 RESEARCH AIRPLANE *

By Joe D. Watts
Flight Research Center

SUMMARY

Severe structural melting damage due to complex shock impingement and interference effects on local aerodynamic heating was experienced on a flight of the X-15-2 research airplane to a maximum Mach number of 6.7. Measured flight temperature data and observed structural damage resulting from shock impingement and interference heating on the airplane and its ablative coating were analyzed in the light of hypersonic wind-tunnel results. The best approximations of the flight results were made by increasing the undisturbed pylon leading-edge heat-transfer coefficient by a factor of 9 and the undisturbed heat-transfer coefficient in the two interference zones by a factor of 7. The calculated effect of increased heat transfer due to interference on radiation-equilibrium temperature is presented for selected hypersonic cruise conditions.

INTRODUCTION

One of the first experiences with actual severe structural damage on a hypersonic aircraft due to a combination of shock impingement and interference effects on local heat transfer occurred on a performance-envelope-expansion flight of the X-15-2 research airplane. The heating damage was near a dummy hypersonic ramjet engine mounted on a pylon (modified ventral fin) at the rear end of the fuselage. The flight, planned to test an ablative coating and evaluate the handling qualities of the airplane with the dummy ramjet installed, reached a maximum Mach number of 6.7 at an altitude of 99,000 feet (30,175 meters). This paper describes the preflight and postflight condition of the aircraft and dummy ramjet engine and the flight conditions. It presents the measured temperature data and an analysis of the flight data made in the light of available wind-tunnel data. The calculated structural radiation-equilibrium temperatures associated with this type of heating condition at selected hypersonic cruise conditions are included to emphasize the effect on radiation-cooled structures.

---

*Title, Unclassified.

SYMBOLS

H	geometric altitude, feet (meters)
h	heat-transfer coefficient, Btu per foot^2-second-degree Rankine (joules per meter^2-second-degree Kelvin)
M	Mach number
p	pressure, pounds per foot^2 (newtons per meter^2)
q	dynamic pressure, pounds per foot^2 (newtons per meter^2)
T	temperature, degrees Fahrenheit (degrees Kelvin)
V	free-stream velocity, feet per second (meters per second)
x	flow length, feet (meters)
α	angle of attack, degrees
ϵ	emissivity

Subscripts:

i	impact
l	local
o	undisturbed
r	recovery
re	radiation equilibrium
t	total
∞	free stream

AIRCRAFT CONFIGURATION

The flight configuration of the modified X-15-2 airplane is shown in figure 1, and the preflight condition of the dummy ramjet engine and pylon is shown in figure 2. The entire pylon and most of the dummy ramjet engine were coated with ablative material for thermal protection. The conical flow-field probes shown in figure 2 were installed to measure flow angularity and pressure levels in the ramjet intake area. The ablative materials were the same as those used in the coating for the entire airplane, MA-25s sprayable silicone ablator on skin surfaces and ESA-3560-IIA pre-molded silicone

ablator in stagnation areas (ref. 1). Figure 3 shows the ablative materials used and the skin thicknesses in the pylon and ramjet-engine area.

Except for a 29-inch (73.66-centimeter) fuselage extension, which was added at the center of gravity, the modified X-15-2 external geometry is essentially the same as that of the basic X-15 airplane. The physical characteristics of the basic airplane are given in reference 2.

INSTRUMENTATION

All instrumentation on the dummy ramjet engine and pylon was installed for developmental tests of the ramjet engine and not for heating investigations. The measurements from which data in this report were obtained were limited to a pylon leading-edge temperature and 10 impact pressures (see fig. 4). The temperature was measured with a chromel-alumel thermocouple spot-welded to the inner surface of the leading edge. The temperature data were recorded on an oscillograph onboard the airplane. The impact pressures were recorded with an onboard manometer. Measurements were made up to about 160 seconds after launch, when the instrumentation wiring in the pylon burned through.

The instruments and methods used in determining geometric altitude, free-stream velocity, dynamic pressure, and angle of attack are described in detail in reference 3.

FLIGHT CONDITIONS

The flight was initiated with the X-15-2 airplane in the maximum performance configuration with design ablative coating and external propellant tanks. The airplane was launched from a B-52 carrier aircraft at a Mach number of 0.82 and a geometric altitude of 45,000 feet (13,716 meters) over Mud Lake, Nev. External propellant tanks were jettisoned at Mach 2.2 and 72,300 feet (22,037 meters) altitude, and the airplane accelerated to Mach 6.7 at 99,000 feet (30,175 meters) altitude. The heating damage to the pylon and dummy ramjet engine occurred at approximately the time of aircraft rocket-engine shutdown. The dummy engine remained attached to the X-15-2 until the airplane had decelerated to approximately Mach 1 in the approach pattern at Edwards Air Force Base. At this point, the dummy ramjet engine separated prematurely. The recovery parachute did not deploy, and the engine impacted on the Edwards bombing range. The airplane made a normal landing. The history of pertinent flight parameters is shown in figure 5. Figure 6 shows the dummy ramjet engine after impact, and figures 7(a), (b), and (c) show the melting damage on the pylon.

AERODYNAMIC-HEATING ANALYSIS

Shock Impingement

Wind-tunnel measurements of the magnitude of the heating effect of shock impingement on a cylindrical leading edge indicate increases from 2 to 10 times the normal

stagnation heating outside the shock-impingement zone (undisturbed). Generally, these levels have been measured in the impingement zone of the vortex sheet which emanates from the intersection of the impinging shock and the leading-edge bow shock. A sketch of a typical shock impingement on a leading edge is shown in figure 8.

References 4 to 8 indicate that when shock impingement occurs near the reattachment point of a separated flow region or near the origin of an attached boundary layer, the local heating is from 5 to 10 times the undisturbed level. When there is no flow separation and the shock impingement occurs after the attached leading-edge flow is well developed, the increase in heating is in direct relation to the increase in pressure and can be predicted by either laminar or turbulent infinite-cylinder boundary-layer theory (refs. 7 and 8).

The highest heating rates due to shock impingement occur when the leading edge is unswept. Sweeping the leading edge tends to relieve flow separation and the related extreme heating condition that results from combining shock impingement and flow reattachment. However, even with highly swept leading edges, the heating rate can be 4 to 6 times the undisturbed laminar level because of the increase in pressure and the transition of the boundary layer to turbulent flow caused by the impinging shock.

The shock pattern in the X-15 ramjet—pylon area is extremely complex. A postulated shock pattern is shown in figure 9. The shocks generated by the ramjet spike tip, spike flare, cowl lip, and bottom impact-pressure probe interact in the general area of the ramjet—pylon junction. It appears from postflight inspection that the four lower impact-pressure probes failed at the root because of very high temperatures and resultant loss of strength or melting at the root. The times at which probe failures occurred are not known; therefore, the exact shock patterns at any particular time cannot be determined. The general levels of the impact-pressure ratios measured with the pylon leading-edge probes are shown in figure 10. The higher values of $\frac{p_{i,l}}{p_{i,\infty}}$ near the cowl lip show that the shock-impingement zone is relatively close to the cowl lip over a wide range of Mach number.

The rearward-facing step of the conical flow-field probe is believed to act as a boundary-layer trip and essentially assure turbulent flow over the entire spike. If turbulent flow is assumed, it is unlikely that any flow separation occurred on the spike except at the lip and pylon corners, as shown in figure 9. Reference 9 indicates that for a similar flare angle and Mach number in turbulent flow, no separation occurs in the vicinity of the flare.

The most severe melting damage was on the leading edge near the bottom impact-pressure probe. Since the shape of the pylon—cowl-lip area cannot be directly compared with the idealized configurations tested in references 4 to 8, it is difficult to attribute the heat-transfer increase to any one of the possible effects observed in the wind-tunnel tests. In order to make a qualitative comparison with the tunnel results, however, the calculated undisturbed heat-transfer coefficient was increased by a factor to match the measured substrate (skin beneath the ablator) temperature data. This factor included the effects of all sources that may have contributed to the heating increase, such as increased pressure, vortex impingement, and boundary-layer reattachment. No attempt is made in this report to isolate a primary contributor. The factor was applied to infinite-cylinder laminar boundary-layer theory assuming an

ablator leading-edge radius of 0.825 inch (2.10 centimeters) and free-stream conditions ahead of the leading edge to obtain the cold-wall heat-flux time history for the flight. This calculated heat input was then used in the NASA Langley Research Center charring-ablator computer program (ref. 10) to compute the substrate temperature up to the time in the flight when the ablator in the impingement zone was consumed. Because of expected scouring action in the shock-impingement zone, the assumption was made that the charred ablator was removed immediately as it was formed so that the virgin ablator was constantly exposed to the stream. The actual leading-edge radius in the shock-impingement zone at any time during the first part of the flight was not known, and it was assumed to remain constant at the initial value of 0.825 inch (2.10 centimeters) until the ablator burned through. By using the calculated substrate temperature at the time of ablator burn-through in the shock-impingement zone as the initial temperature, the temperature time history of the exposed leading edge with a 0.375-inch (0.953-centimeter) radius was then calculated for the remainder of the flight. The calculated temperature time history of the leading edge in the shock-impingement zone is compared with the measured leading-edge temperature in figure 11. The primary objective in comparing the calculated temperature in the shock-impingement zone with the nearest available measured temperature was to match the ablator burn-through time (about 140 seconds from launch) by increasing the undisturbed pylon stagnation line heat-transfer coefficient by known factors. The match of the ablator burn-through time as shown in figure 11 was obtained with a factor of 9. The difference of the slopes of the measured and the calculated data after burn-through can be attributed to the location of the thermocouple outside the shock-impingement zone. The figure shows that the calculated leading-edge temperature increased rapidly to near radiation-equilibrium temperature after ablator burn-through.

Interference Heating

The ablator was completely eroded away on the bottom of the fuselage around the pylon leading edge. The bare fuselage skin can be seen in figure 7. Some permanent skin deformation resulted.

The fuselage/pylon leading-edge configuration is similar to a flat plate with an attached circular cylinder of zero sweep. It has been shown (ref. 11) that flat-plate heating rates in the proximity of a plate/cylinder junction can be 7 to 8 times the undisturbed level. Therefore, a factor of 7 times the turbulent flat-plate heat-transfer coefficient using the flow length of 40.45 feet (13.56 meters) was used in an attempt to calculate the substrate temperature time history. The calculated cold-wall heat-flux time history was used as an input to the charring-ablator computer program to determine the substrate temperature and the probable time at which the ablator was completely removed, assuming immediate char removal. When the ablator was removed, the skin temperature time history was continued through the remainder of the flight by using a "thin-skin" calculation. Since no data were obtained at this location, the calculated temperature shown in figure 12 represents the best estimate of what occurred in flight. It appears that the calculated heat-transfer coefficient, increased by a factor of 7, resulted in a substrate temperature that corresponded favorably with the observed condition of the structure. The 1400° F (1034° K) temperature would have been sufficient to cause the observed permanent skin buckling in the fuselage interference zone, but the temperature was far below the melting point of Inconel X.

The other area that experienced interference heating was the ramjet cowl lip, which was influenced by the presence of the pylon. The flow length was short compared with that of the fuselage interference zone, and the thin boundary layer coupled with the interference effect of the pylon leading edge resulted in extremely high temperatures. Figure 13 shows the cowl-lip temperature time history calculated by using the same factor of 7 that was used on the fuselage to account for the interference effects. The protection afforded by a very thin spray coat of ablator was neglected. The calculated temperature exceeded the melting point of the 4130 steel structure (2795° F (1810° K)) for a short time, as the damage shown in figure 6 indicates.

GENERAL COMMENTS

It was shown in figure 11 that the calculated substrate temperature of the pylon leading edge rapidly approached the radiation-equilibrium temperature after ablator burn-through, even though the flight conditions were highly transient. Because the large increases in heat transfer result in localized temperatures near radiation equilibrium, it is of interest to note the effect of increasing heat transfer on the level of radiation-equilibrium temperature. Figure 14 shows this effect over a range of hypersonic velocities for a selected stagnation area and free-stream dynamic-pressure level. As shown, an accurate value of the heating increase over the undisturbed level $\frac{h}{h_o}$, even for the higher velocities, becomes somewhat academic at values of $\frac{h}{h_o}$ greater than 4. At the high velocities and high values of $\frac{h}{h_o}$, temperature limits of available metals such as those shown in the figure would dictate a departure from radiation-cooled structure design toward another approach, such as active cooling, unless some means of reducing heating, possibly by increasing the leading-edge radius and sweep angle, could be introduced into the design.

The radiation-equilibrium temperature levels encountered with a flat plate, shown in figure 15, are much lower than in a stagnation region. The applicability of radiation-cooled structural design to nonstagnation surface areas, even in interference zones, would seem to be within the present state of the art of materials except in areas very near the leading edge.

CONCLUDING REMARKS

Severe structural melting damage due to complex shock impingement and interference heating was experienced on a flight of the X-15-2 research airplane to a maximum Mach number of 6.7.

Postflight calculations of structural temperatures for the actual flight conditions were made, utilizing wind-tunnel shock-impingement and interference-heating measurements, and compared with measured temperature data and the observed postflight physical condition of the structure and ablative coating. The best approximations of the flight results were made by increasing the undisturbed pylon leading-edge heat-transfer coefficient by a factor of 9 and the undisturbed heat-transfer coefficient in the two interference zones by a factor of 7.

The X-15-2 incident emphasizes the need for extreme care in the design of hypersonic vehicles where shock impingement and interference effects are present because of the extremely high temperatures encountered. For the stagnation case with shock impingement, temperatures may even exceed the limits of such high-performance metals as columbium, tantalum, and tungsten, unless the external geometry of the structure can be designed to minimize aerodynamic heating.

Flight Research Center,
National Aeronautics and Space Administration,
Edwards, Calif., June 7, 1968,
719-01-00-03-24.

REFERENCES

1. Price, A. B: Design Report - Thermal Protection System X-15A-2. Martin Marietta Corp. (NASA CR-82003), 1968.

2. Gord, P. R.: Measured and Calculated Structural Temperature Data From Two X-15 Airplane Flights With Extreme Aerodynamic Heating Conditions. NASA TM X-1358, 1967.

3. Webb, Lannie D.: Characteristics and Use of X-15 Air-Data Sensors. NASA TN D-4597, 1968.

4. Newlander, Robert A.: Effect of Shock Impingement on the Distribution of Heat-Transfer Coefficients on a Right Circular Cylinder at Mach Numbers of 2.65, 3.51, and 4.44. NASA TN D-642, 1961.

5. Bushnell, Dennis M.: Effects of Shock Impingement and Other Factors on Leading-Edge Heat Transfer. NASA TN D-4543, 1968.

6. Hiers, Robert S.; and Loubsky, William J.: Effects of Shock-Wave Impingement on the Heat Transfer on a Cylindrical Leading Edge. NASA TN D-3859, 1967.

7. Beckwith, Ivan E.: Experimental Investigation of Heat Transfer and Pressures on a Swept Cylinder in the Vicinity of Its Intersection With a Wedge and Flat Plate at Mach Number 4.15 and High Reynolds Numbers. NASA TN D-2020, 1964.

8. Bushnell, Dennis M.: Interference Heating on a Swept Cylinder in Region of Intersection With a Wedge at Mach Number 8. NASA TN D-3094, 1965.

9. Becker, John V.; and Korycinski, Peter F.: Heat Transfer and Pressure Distribution at a Mach Number of 6.8 on Bodies With Conical Flares and Extensive Flow Separation. NASA TN D-1260, 1962.

10. Swann, Robert T.; Pittman, Claud M.; and Smith, James C.: One-Dimensional Numerical Analysis of the Transient Response of Thermal Protection Systems. NASA TN D-2976, 1965.

11. Burbank, Paige B.; Newlander, Robert A.; and Collins, Ida K.: Heat-Transfer and Pressure Measurements on a Flat-Plate Surface and Heat-Transfer Measurements on Attached Protuberances in a Supersonic Turbulent Boundary Layer at Mach Numbers of 2.65, 3.51, and 4.44. NASA TN D-1372, 1962.

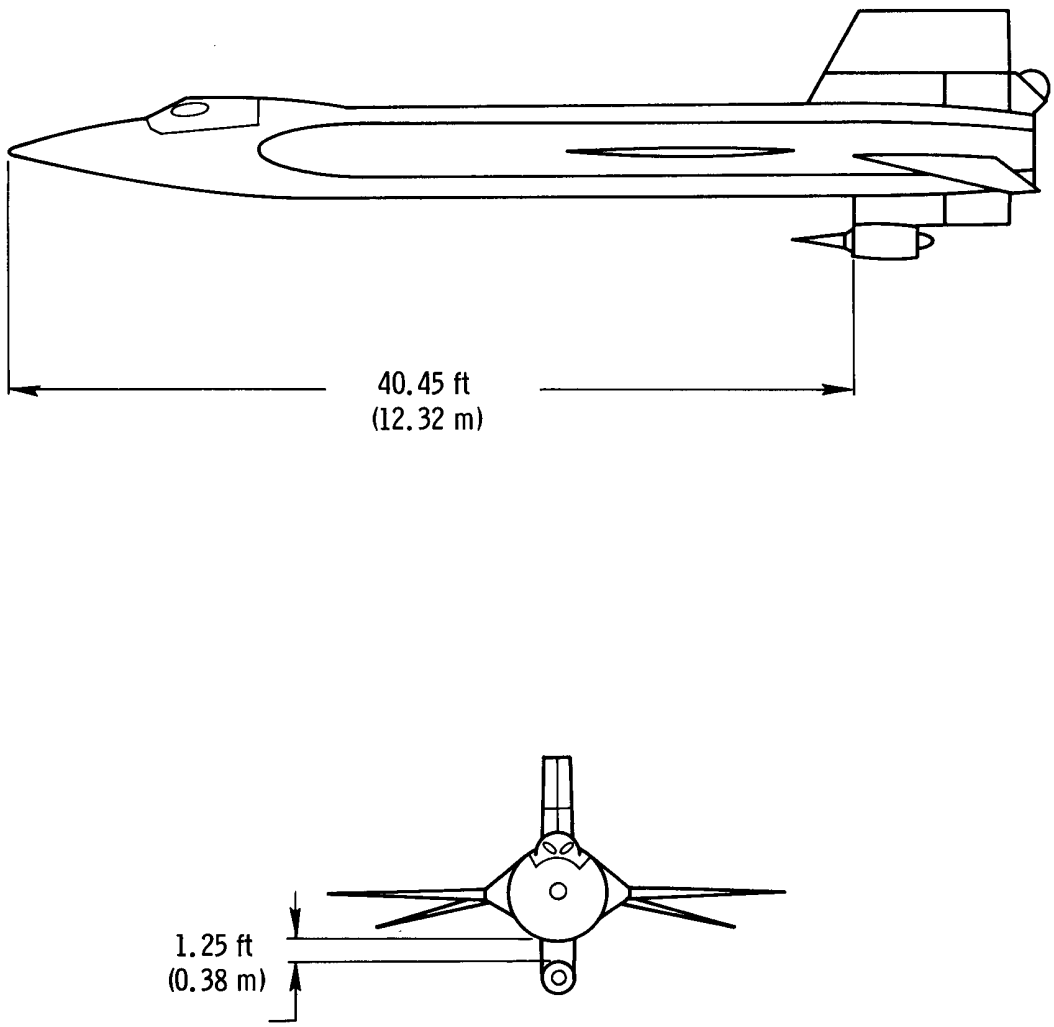

Figure 1. – Two-view sketch of the X-15-2 airplane with dummy ramjet engine installed (after jettison of external propellant tanks).

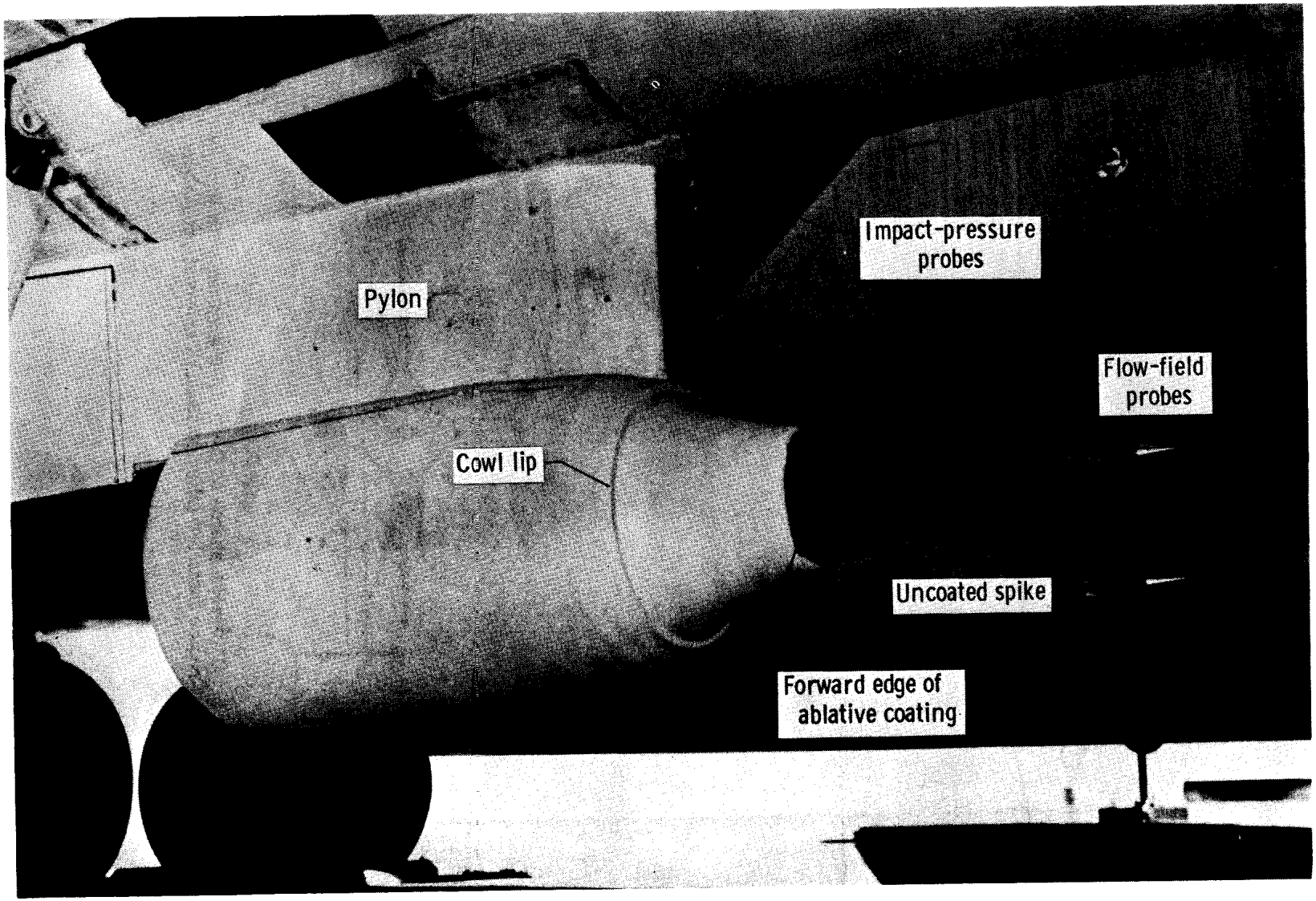

E-17493

Figure 2. – Preflight condition of dummy ramjet engine and pylon.

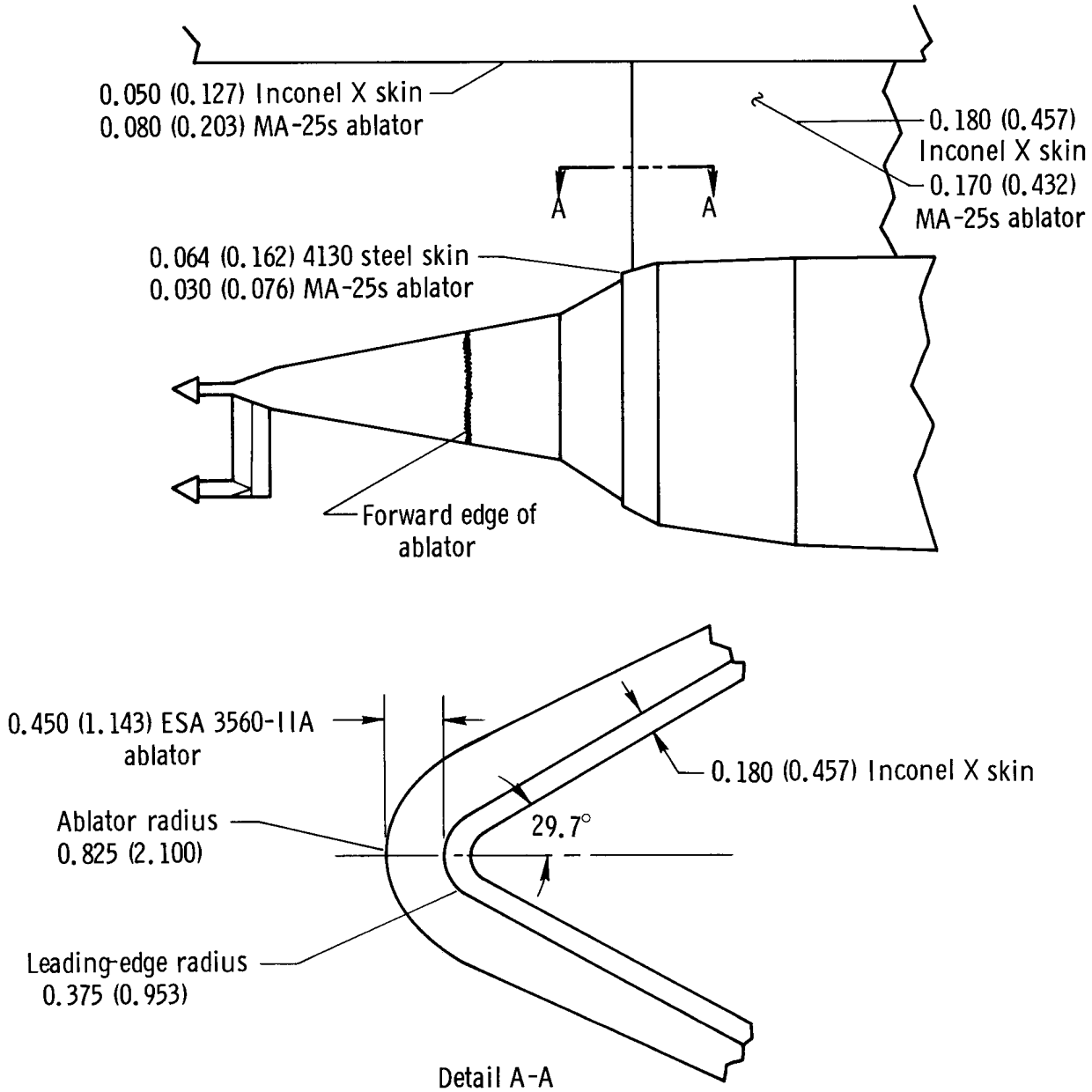

Figure 3. – Skin and ablator thicknesses in the shock impingement and interference heating zones. Dimensions in inches (centimeters) unless otherwise noted.

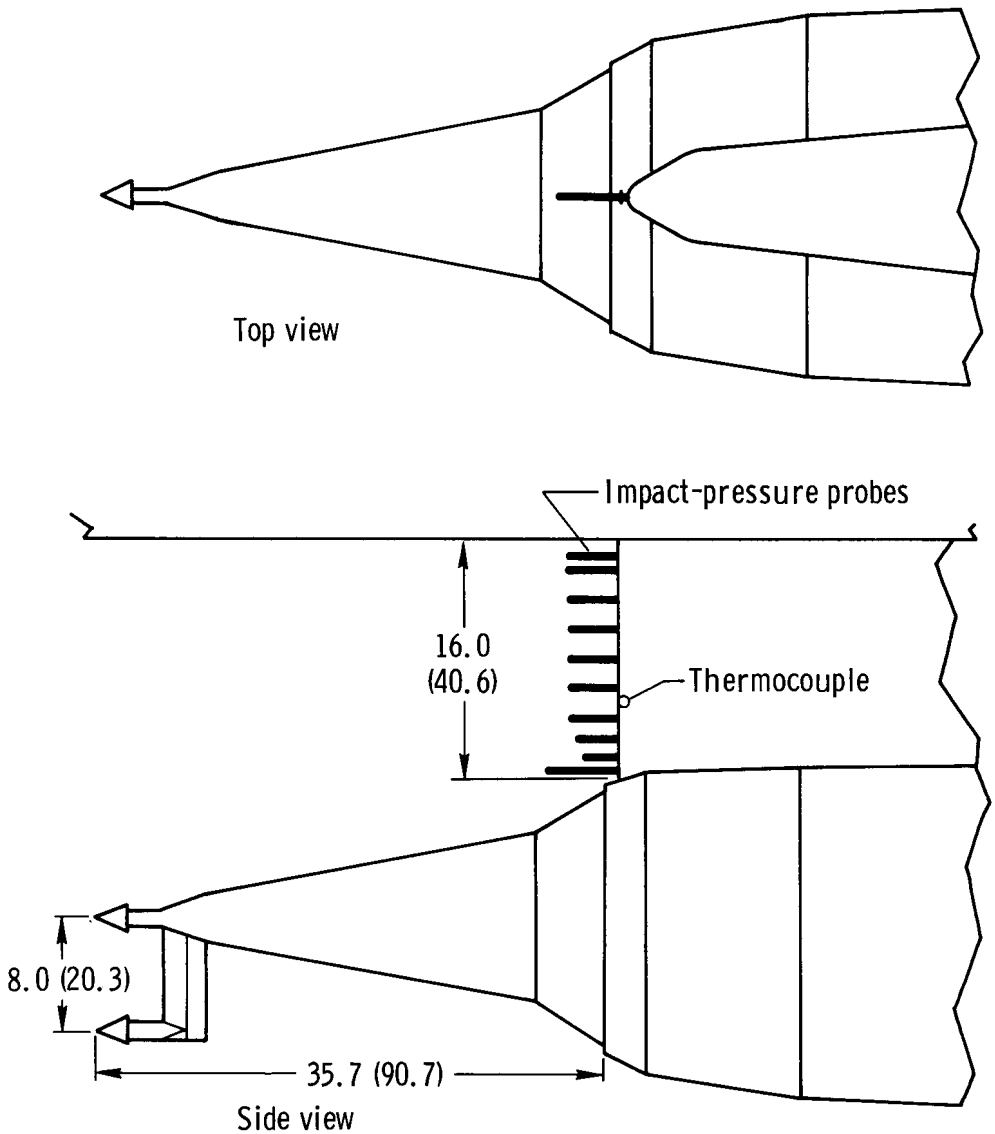

Figure 4.– Dummy ramjet engine and pylon with pertinent instrumentation. Dimensions in inches (centimeters).

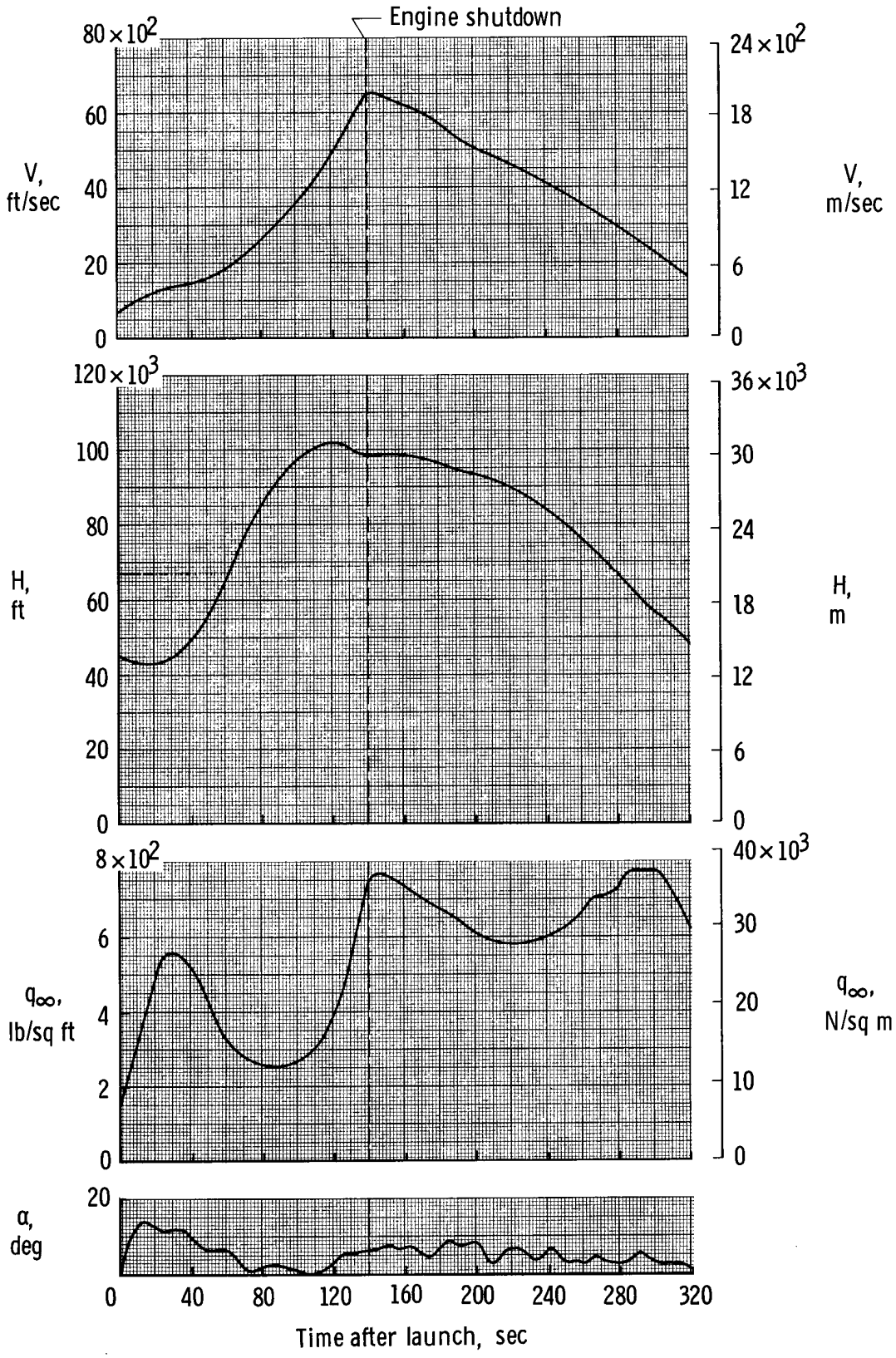

Figure 5. – History of pertinent flight parameters.

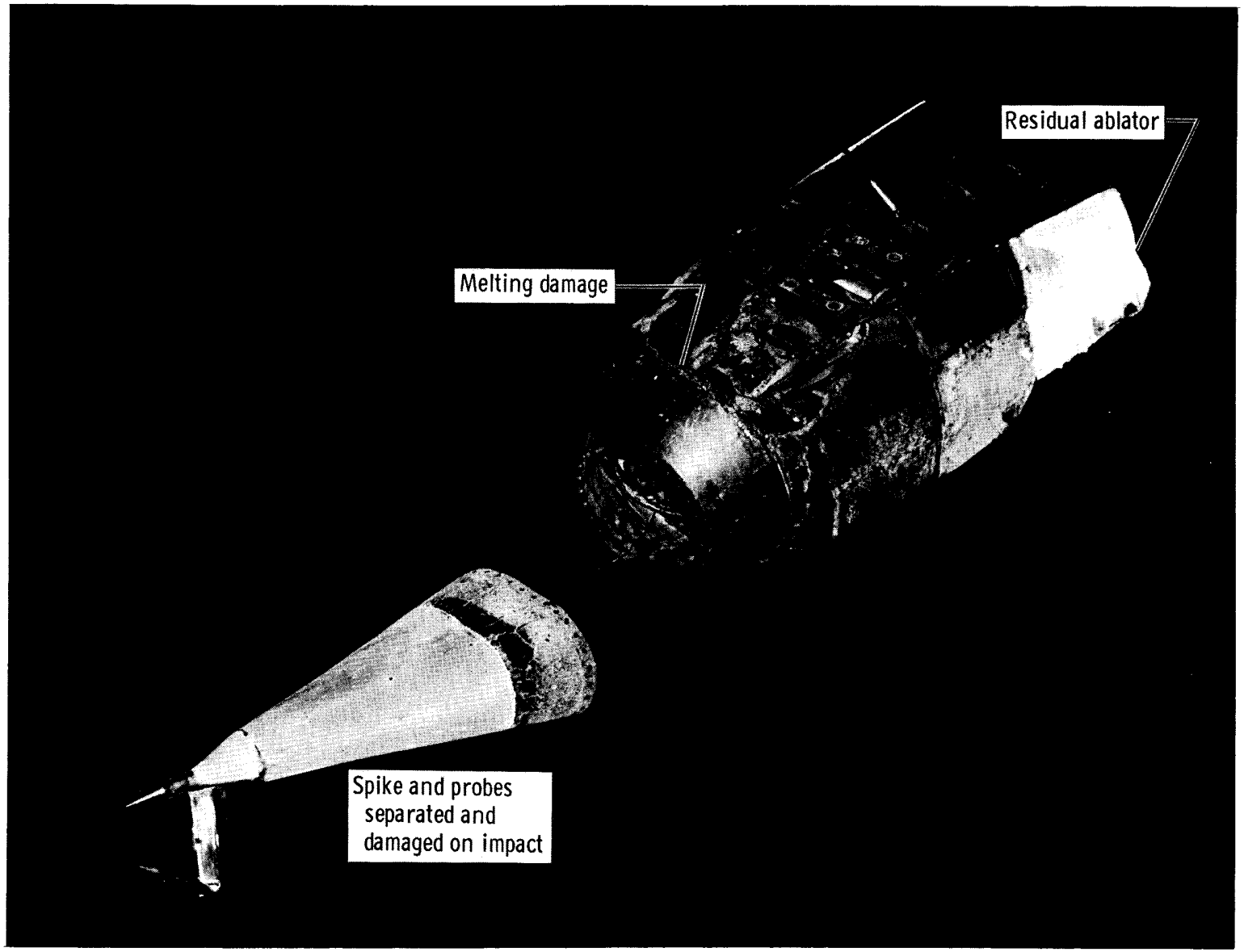

E-17534

Figure 6. – Postflight condition of dummy ramjet engine.

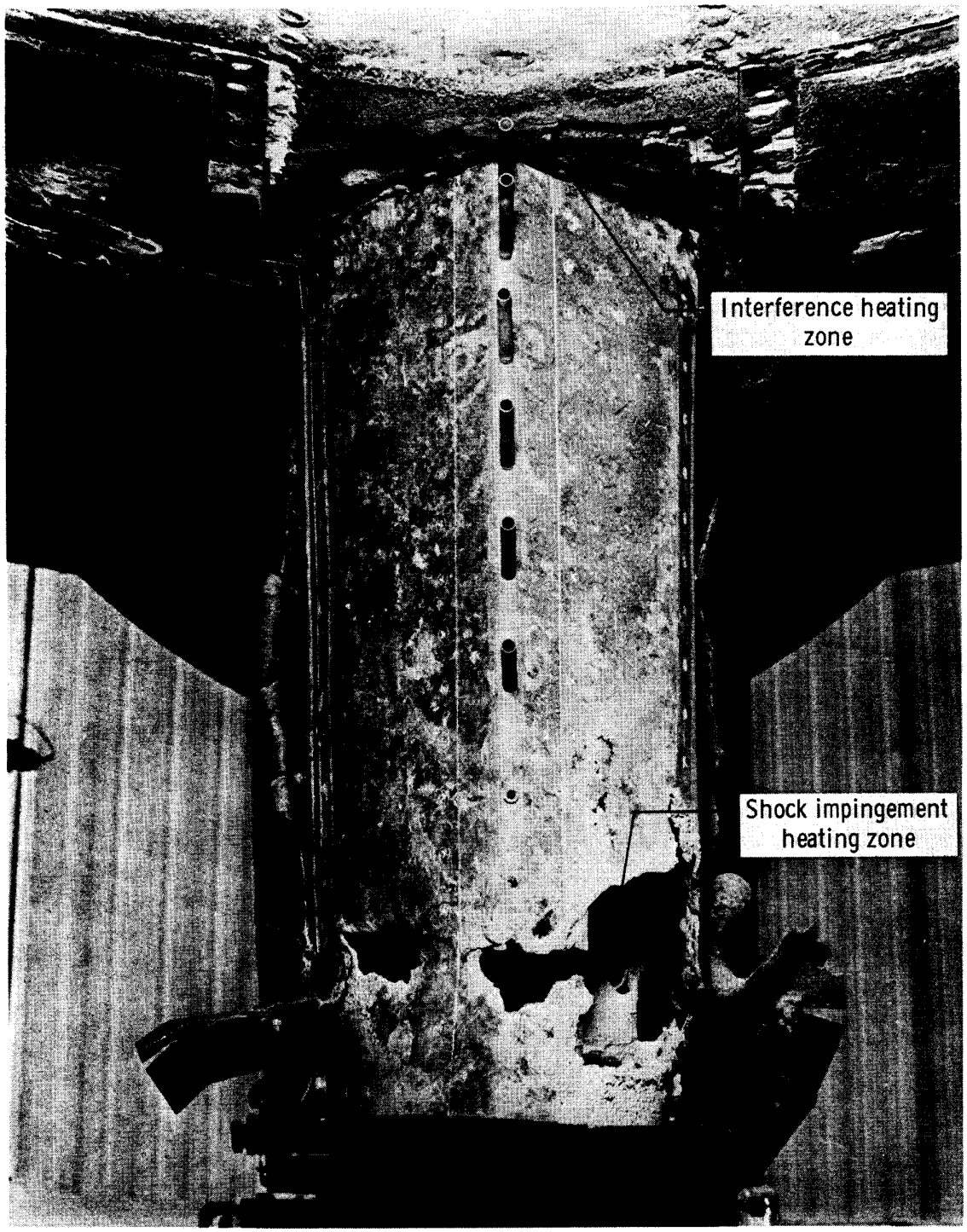

E-17525

(a) Front view.

Figure 7. – Postflight condition of dummy ramjet engine pylon.

(b) Left side view.

E-17526

Figure 7. – Continued.

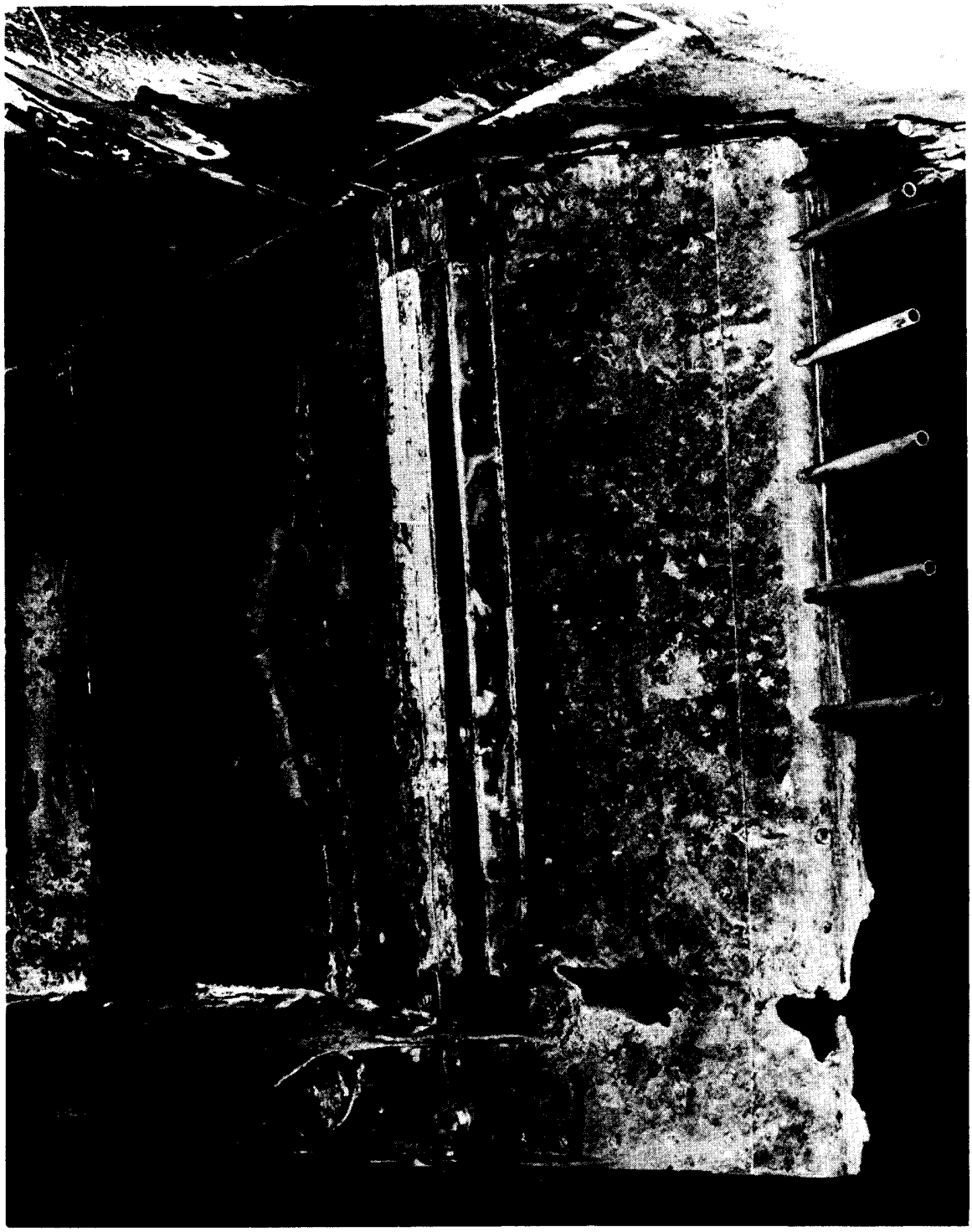

E-17527

(c) Right side view.

Figure 7. – Concluded.

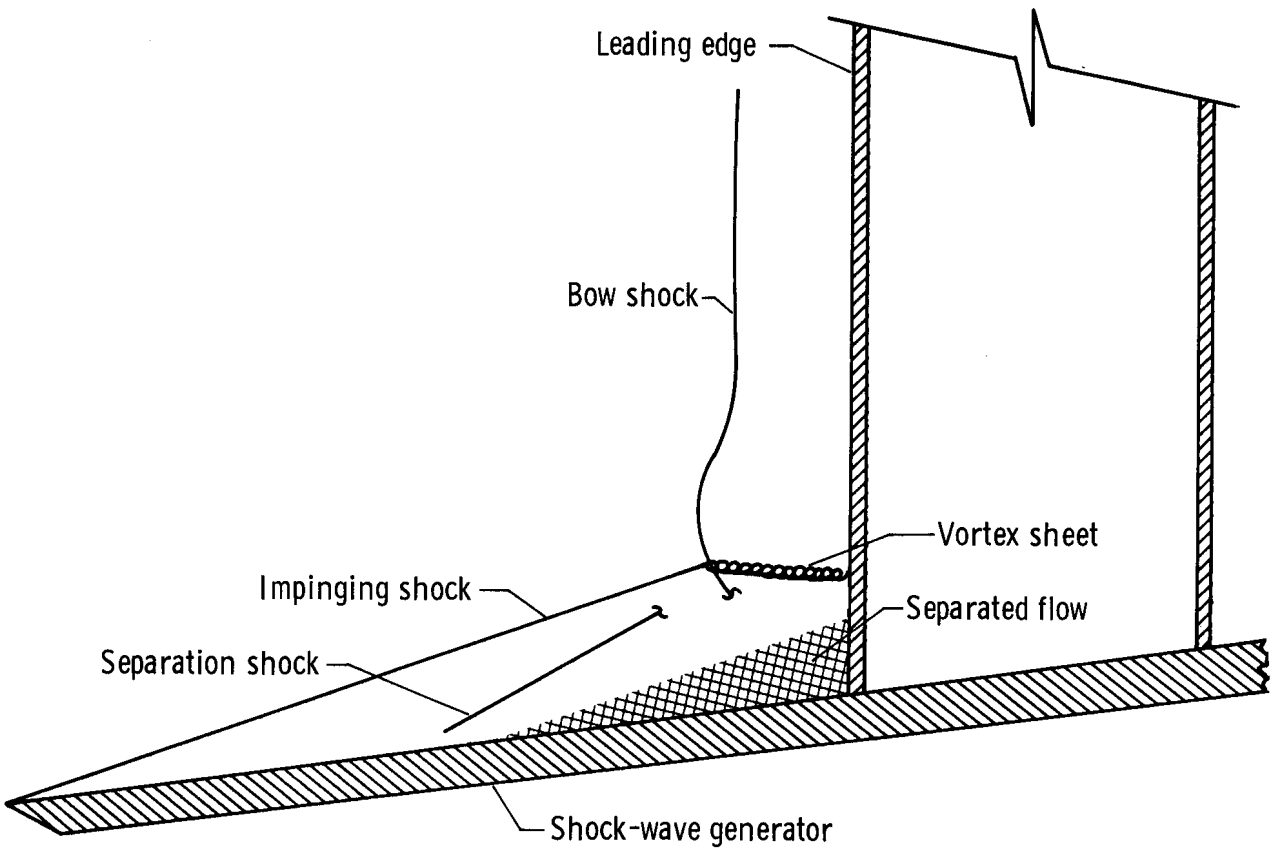

Figure 8. – Flow field associated with leading-edge shock impingement (adapted from ref. 4, appendix A).

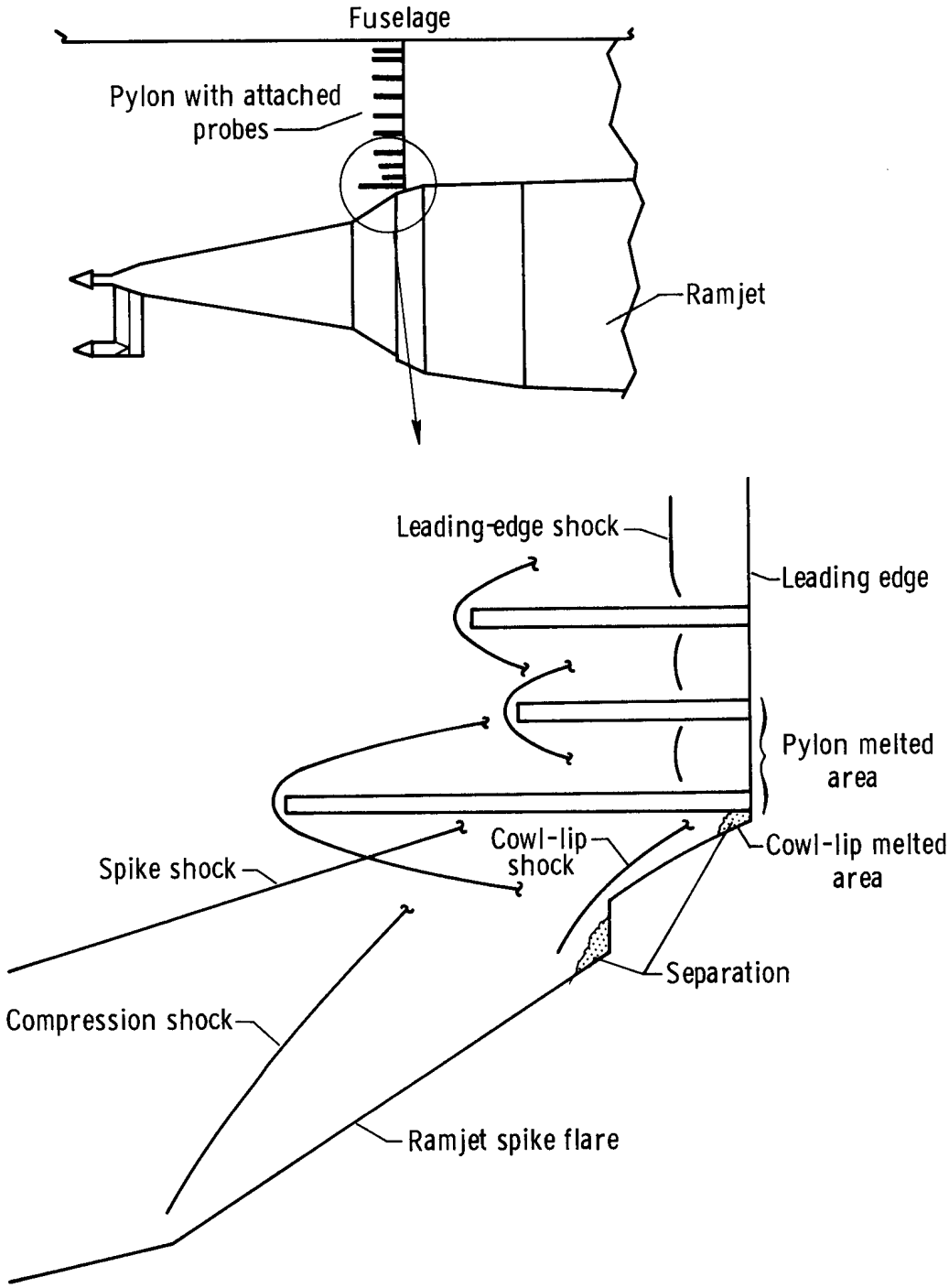

Figure 9. – Assumed shock patterns in shock impingement and cowl-lip interference zones.

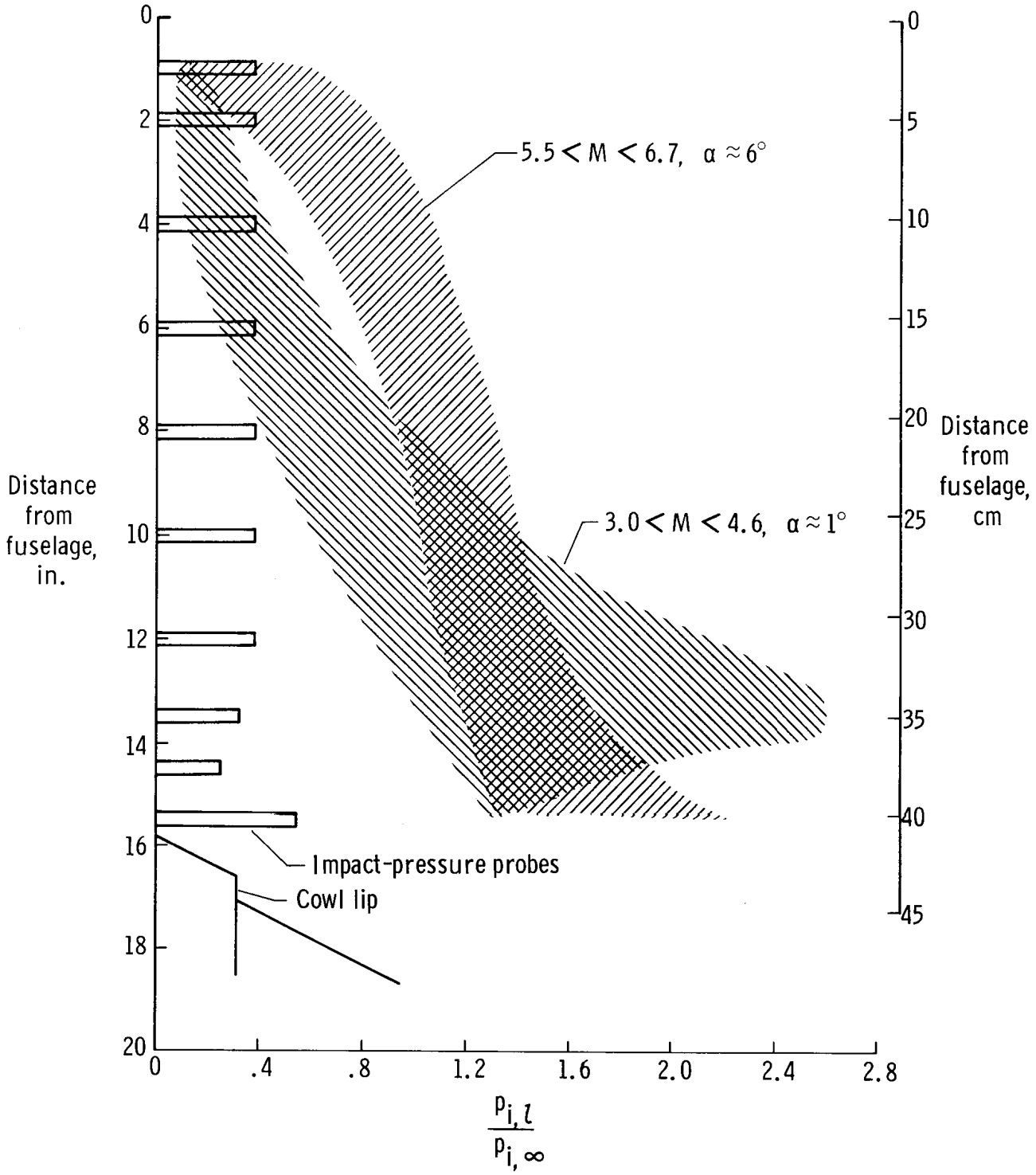

Figure 10.– Impact-pressure-ratio distribution on the pylon leading edge for two Mach number ranges.

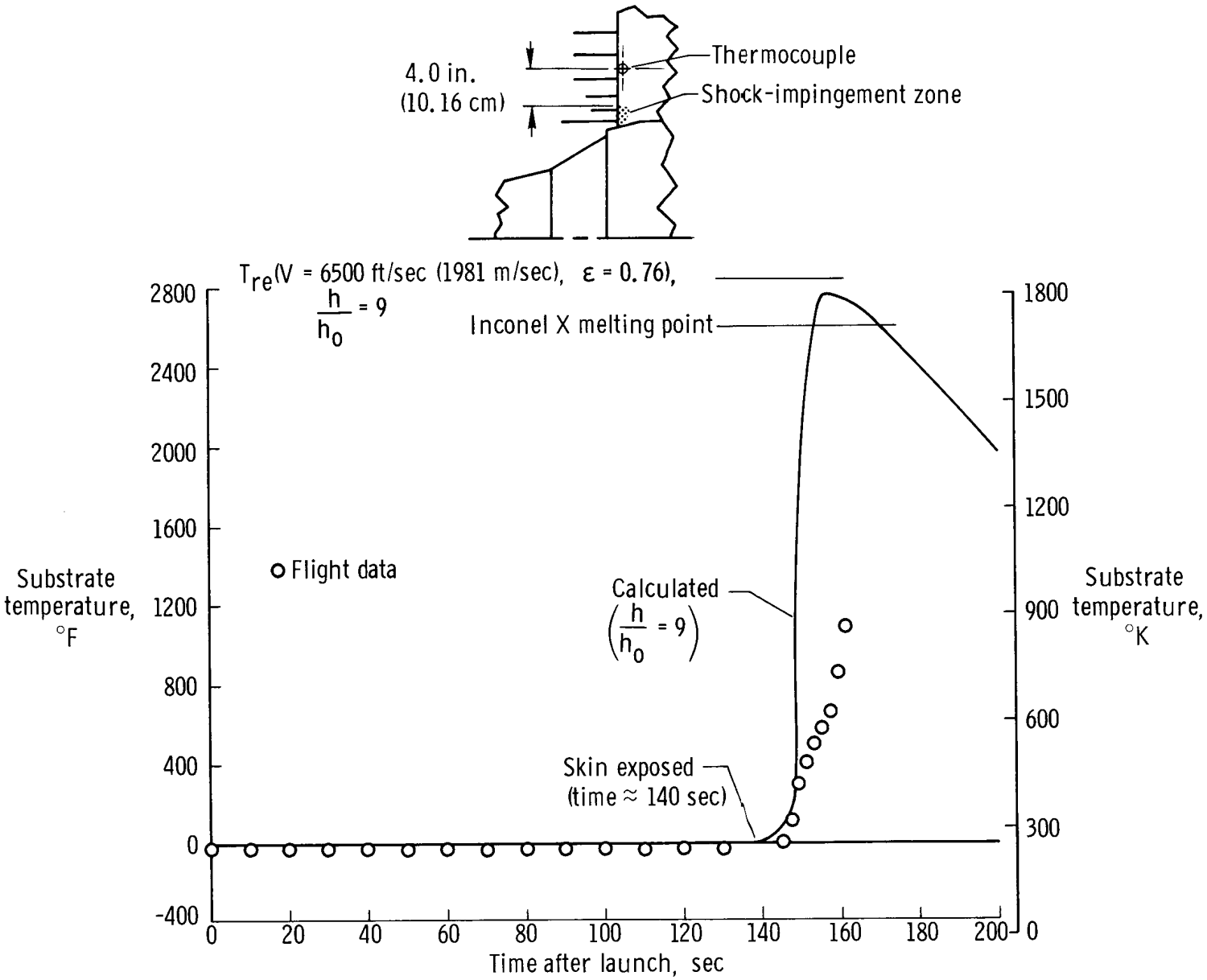

Figure 11. – Calculated substrate temperature time history in shock impingement zone compared to nearest measured temperature.

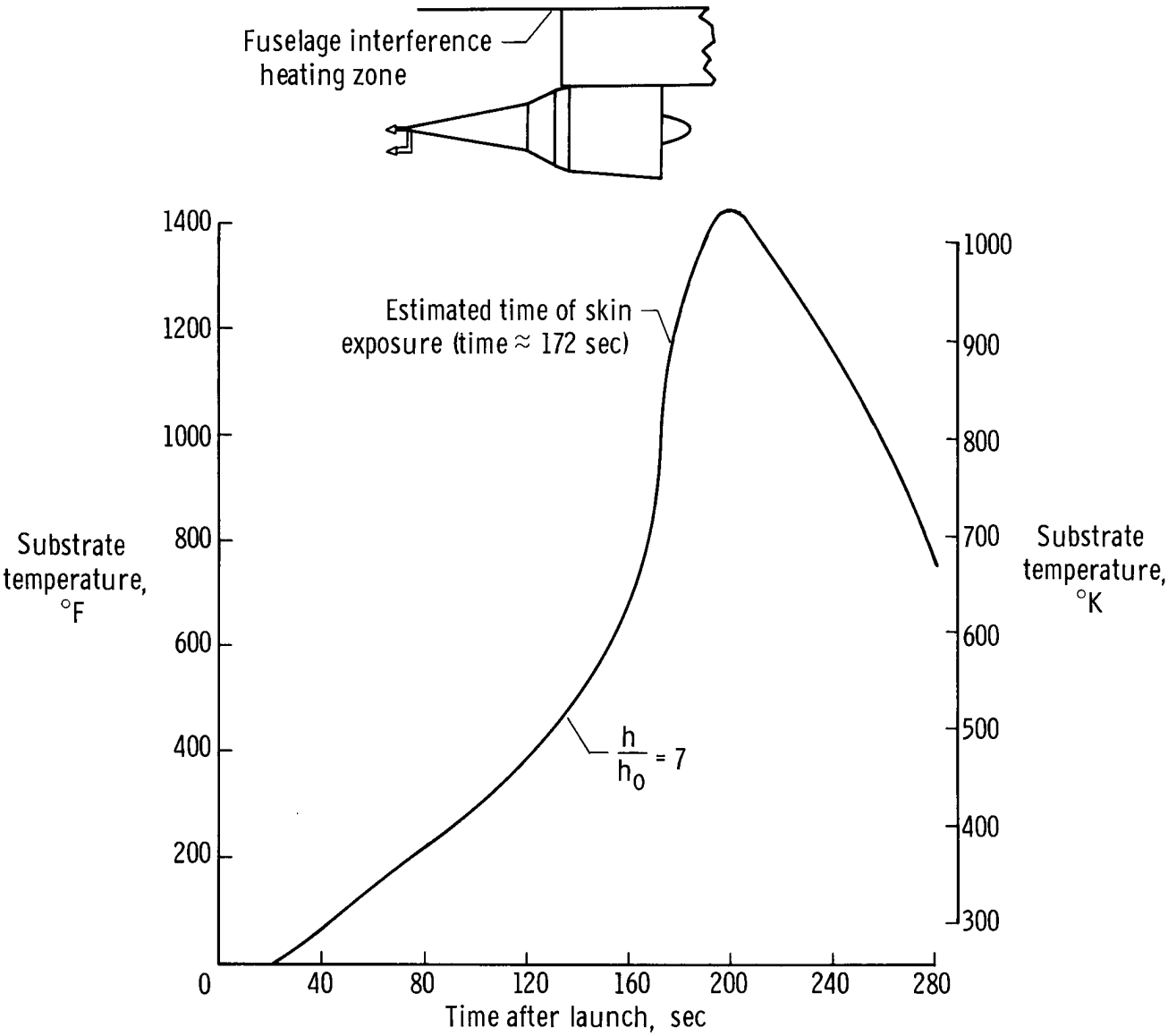

Figure 12. – Calculated substrate temperature time history of fuselage interference heating zone.

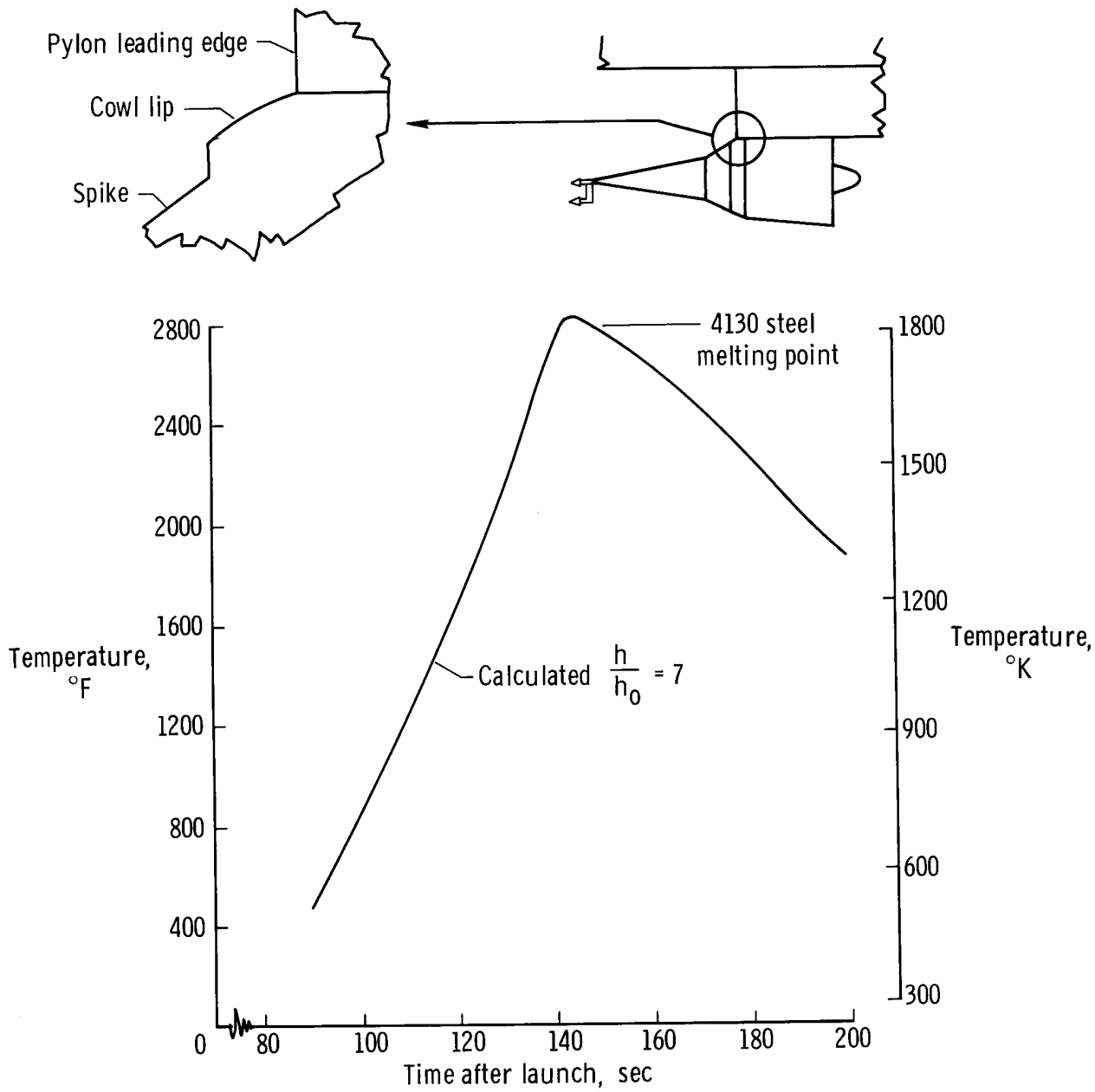

Figure 13. – Calculated temperature time history of cowl-lip interference zone.

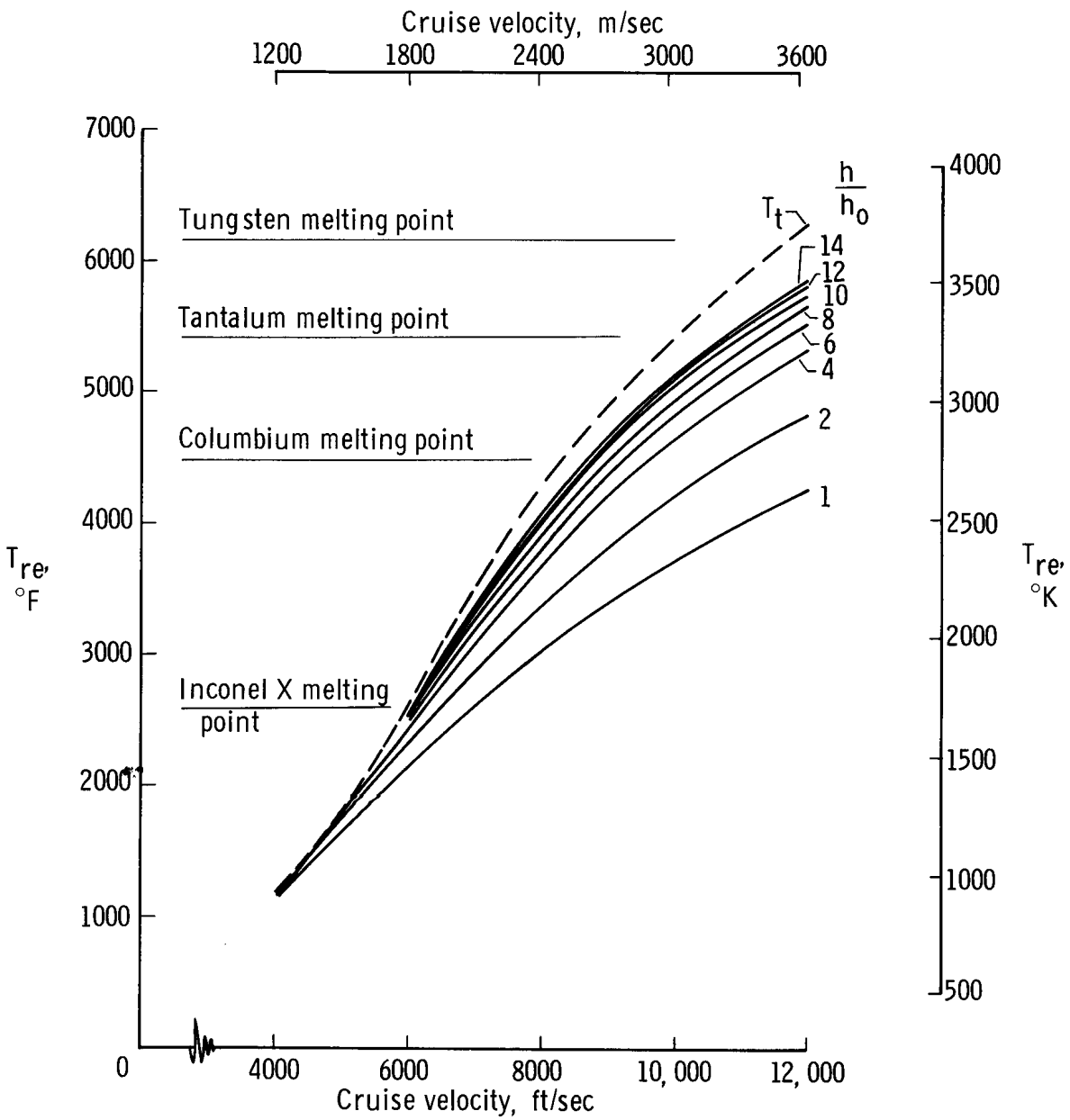

Figure 14. – Effect of increasing laminar heat-transfer coefficient on radiation-equilibrium temperature for a 0.5-inch- (1.27-centimeter-) radius leading edge with zero sweep. $q_\infty = 1000$ lb/ft^2 (47,880 N/m^2); $\epsilon = 0.85$.

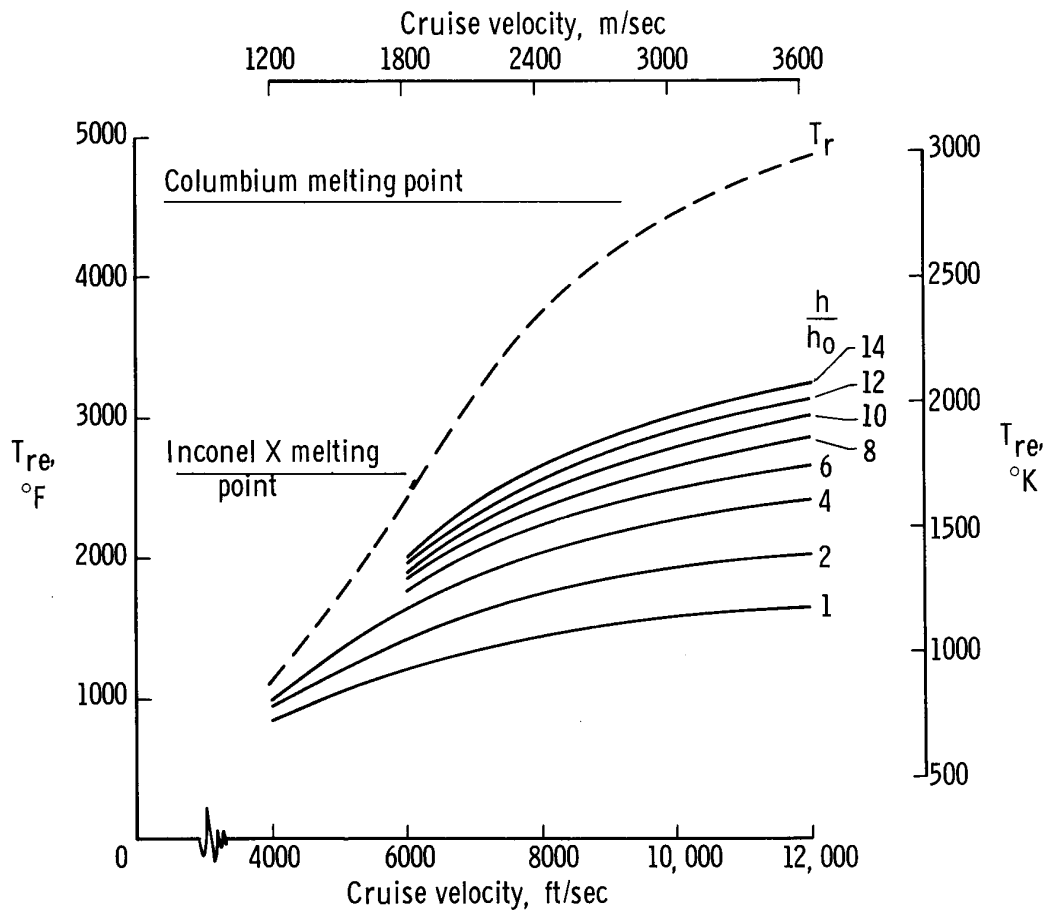

Figure 15. – Effect of increasing turbulent heat-transfer coefficient on radiation-equilibrium temperature for a flat plate at zero angle of attack. q_∞ = 1000 lb/ft^2 (47,880 N/m^2); x = 10 ft (3.05 m); ϵ = 0.85.